An integrated solution for lane level irregular driving detection on highways

Rui Sun *, Washington Yotto Ochieng, Shaojun Feng

Center for Transport Studies, Imperial College London, SW7 2AZ, United Kingdom

A b s t r a c t

Global Navigation Satellite Systems (GNSS) has been widely used in the provision of Intelligent Transportation System (ITS) services. Current meter level system availability can fulfill the road level applications, such as route guide, fleet management and traffic control. However, meter level of system performance is not sufficient for the advanced safety applications. These lane level safety applications requires centimeter/decimeter positioning accuracy, with high integrity, continuity and availability include lane control, collision avoidance and intelligent speed assistance, etc. Detecting lane level irregular driv-ing behavior is the basic requirement for these safety related ITS applications. The two major issues involved in the lane level irregular driving identification are accessing to high accuracy positioning and vehicle dynamic parameters and extraction of erratic driving behaviour from this and other related information. This paper proposes an integrated solu-tion for the lane level irregular driving detection. Access to high accuracy positioning is enabled by GNSS and Inertial Navigation System (INS) integration using filtering with precise vehicle motion models and lane information. The detection of different types of irregular driving behaviour is based on the application of a Fuzzy Inference System (FIS). The evaluation of the designed integrated systems in the field test shows that 0.5 m accu-racy positioning source is required for lane level irregular driving detection algorithm and the designed system can detect irregular driving styles.

1. Introduction

Traffic safety plays an important role in modern society. In 2012, the total casualties in road accidents was 195,723, of which 1754 were killed and 23,039 were serious injuries (Kilbey, 2013). Abnormal driving maneuvers, including sudden lane change and erratic driving due to drowsiness, resulting in more than 90 percent of these accidents (Aljaafreh, 2012). From National Highway Traffic Safety Administration (NHTSA), these irregular driving styles could be characterized as weaving, swerving and jerky driving. If early detection and warning of irregular driving can be provided, the probability of the accident happen will be reduced. Intelligent Transport Systems (ITS) technologies can be applied to realize irregular driving identification, with the function of evaluating driving performance, improving driving behaviour and have potential benefits for lane control and collision avoidance applications.

In the recent years, the researches for the irregular driving detection in the early stage are mainly based on the vehicle's real-time driving pattern detection and driver's physical behavior monitoring.

In regard to the researches of vehicle's driving pattern detection, which uses of different sensors including positioning, orientation, velocity and vision to detect vehicle's motion information. The analysis of the collected data is to find cues of irregular driving. Lecce and Calabrese (2008) designed a driving information collection system based on specific sensors and GPS receivers and applied pattern matching algorithm to classify driving styles. Chang et al. (2008) developed a vision based system with the function of learning the trajectories and longitudinal and lateral velocities of the vehicle based on Fuzzy Neural Networks (FNNs) and subsequently calculated the level of danger of the vehicle. Imkamon et al. (2008) devel-oped a vision and orientation sensors based method for detecting dangerous driving behaviours. A fuzzy logic system is subsequently used to classify different levels of hazardous driving. Krajewski et al. (2009) used orientation sensors to collect steering data and extracted driver's fatigue information and then used signal processing to capture fatigue impaired patterns. Dai et al. (2010) developed dangerous vehicle manoeuvres detection system typically associated with drunk driving using a mobile phone with an accelerometer and orientation sensor. The acceleration pattern from sensor readings are matched with the typical drunk driving patterns extracted from real driving tests. Sultani and Choi (2010) developed an algorithm for detecting and localizing irregular traffic based on video image processing using an intelligent driver model. Saruwatari et al. (2012) proposed a vision sensor based method for detecting abnormal driving of vehicles, including meandering, trans-verse motion and sudden acceleration or deceleration. The abnormal vehicle motions can be extracted in the sense of group behaviour by using a multi-linear relationship in space–time images.

In regard to the researches of driver's behaviour monitoring, which mainly uses visual or auxiliary systems to monitor the driver physical behaviour when driving. Visual observation is an option for monitoring and detecting of fatigue driver. Eriksson and Papanikolopoulos (2001) proposed a vision-based approach for diagnosing fatigue driver by monitoring a driver's eyes and issuing a warning when the irregular eye closure is detected. Zhu and Ji (2004) developed a two-camera based method to predict fatigue with a probabilistic model based on the captured visual cues of drivers, such as eyelid movement, gaze movement, head movement and facial expression. Lee et al. (2006) also developed a camera based method to monitor the driving status of the driver. The driver's sight line and driving path are captured by the camera and also the correlation between them is calculated. Omidyeganeh et al. (2011) proposed a scheme for drowsiness driver detection based on a fusion of eye closure and yawning detection methods. A camera installed in the car is used to capture the driver's facial appearance and the signs of driver fatigue are studied. A warning will send to the driver, once the drowsiness driver state is determined.

Auxiliary systems coupled with the vehicle to detect interactions between the driver and the vehicle to indicate drunk driving is also an option for monitoring the driver. Albu et al. (2008) not only used a vision-based system to monitor eye conditions in order to detect fatigue while driving but also used an auxiliary force sensor on the accelerator pedal to collected the exerted force for monitoring driver fatigue. Heitmann et al. (2001) have developed a multi-parametric approach to monitor and prevent driver fatigue based on various auxiliary sensors, including a head position sensor, an eye-gaze system, a two pupil-based system and an in-seat vibration system, for alertness monitoring. Desai and Haque (2006) proposed a system to define the level of driver alertness based on the time derivative of force exerted by the driver at the vehicle–human interface, such as pressure on the accelerator pedal. Sandberg et al. (2011) have proposed a physiological signals based method for abnormal driving detection. The electroencephalography is used to detect brain activity and signs of drowsiness can be extracted by analysing of the signal.

From the discussion of literature above, for the researches of monitoring driver physical behaviour and preventing fatigue or inattention, vision sensors are always used in the vehicle to monitor the driver. Cameras inside of the vehicle are a potential safety hazard to the driver by distracting the driver, also performance of the vision sensors is affected by the ambiguous road marks and bad weather seriously. For auxiliary system based driver physical behaviour monitoring, the compatibility of the system is still a big problem. Furthermore, the complexity and high cost of the system make it difficult to integrate in practice. Most of the research is still on either simulations or laboratory conditions with very few field trials. Even some research teams have addressed field tests, they generally simply describe the field scenarios without detail results comparison or discussion. For the detection of the irregular driving using a vehicle's real-time driving patterns, the approaches in the literature often come with relatively high sensor or computational costs or have some unacceptable drawbacks, in particular some systems are still in an early stage of development without field tests. However, the systems could still be generally improved by improved performance of the positioning and orientation detection technology (Krajewski et al., 2009; Dai et al., 2010).

For all these reasons, it is difficult to realize detection of irregular driving based on driver physical monitoring. However, it is comparatively feasible to realize real-time driving pattern based irregular driving detection and the system performance could be improved based on the positioning improvement. Furthermore, the literature review has shown that none of current algorithms are appropriate for identifying the different types of irregular driving styles. The reason is that the detection performance is currently limited by the availability of high accuracy positioning. Also for the current researches, some are just focused on the GNSS positioning technology improvement and some are only focused on driving pattern recognition but there is rarely a link between the two.

This paper present a work on the GPS and INS integration estimated results to provide high accuracy positioning and dynamic parameters estimation for the FIS based irregular driving identification. The rest of the paper is organized as follows. First, in Section 2, the GPS/INS integration model for the lane level precise positioning and dynamic parameter estimation algorithm that employs Extended Kalman Filter (EKF) and Particle Filter (PF) with relative motion and lane models are presented as well as the comparison of the positioning performance of the fusion models. Section 3 then explains the detection method of driving events that characterize different types of designed driving styles based on FIS using estimated

integrated results. Finally, evaluation of the designed algorithm on the field experiments and the conclusions obtained from them are discussed in Sections 4 and 5.

2. Lane level positioning and precise parameter estimation model

This section describes the lane level positioning and dynamic parameter estimation system based on PF/EKF filters and precise vehicle motion models on straight and curved lanes. The accuracy of positioning and estimated parameters from fusion models are critical for the next section Fuzzy Inference System (FIS) based irregular driving detection. Section 2.1 describes the PF model design and Section 2.2 describes the EKF model design. Section 2.3 shows the comparison of the estimated results from different fusion models for the defined simulation scenarios.

2.1. Particle filter model design

The PF is one of the most applicable filters for sensor fusion. In PF, the probability density is approximated by a number N of weighted samples. The steps of PF based lane level positioning are described as follows (Gustafsson et al., 2002).

2.1.1. Initialization

In the designed GPS/INS fusion based lane level precise positioning algorithm, the defined state vector for PF is in (1),

$$X(t) = (\ xy v\theta\omega a\beta d)^T \tag{1}$$

where

x, is the X-axis coordinate (in metres) of point o in the local UK National Grid coordinate system
y, is the Y-axis coordinate (in metres) of point o in the local UK National Grid coordinate system
v, is the velocity at the heading direction
θ, is the heading angle of the vehicle
ω, is the vehicle yaw rate
a, is the vehicle acceleration along the heading
β, is the angle between the lane segment and the local British National Grid coordinates
d, is the vehicle lateral displacement

The state vector (1) can be divided into two sub state vectors: vehicle motion vector (2) and lane geometry related vector (3). Sub state (2) is for the particle filter cycle calculation and sub state vector (3) is the dependent vector of state vector (2) in the calculation.

$$p(t) = (\ xy v\theta\omega a)^T \tag{2}$$

$$q(t) = (\ \beta d)^T \tag{3}$$

In the particle filter operation, the parameters change with time epochs and particles with each parameter within the state vector (1) will be expression as.

$$X^i_t(t = 0 \ldots n; i = 1 \ldots n) \tag{4}$$

where

X^i_t, is the parameter within the state vector (1) on the time epoch t with the particle number i.

The filter begins with the initialization of the particles $x^i{}_0$ of the vehicle motion vector $p(t)$. To realize this, first the local coordinate sub-state variables x and y are randomly generated following a Gaussian distribution with the first accepted GPS point as the mean value and a standard deviation value according to the GPS a posteriori solution statistics. The initial heading velocity $v^i{}_o$ is set as 0, for the initial position of the vehicle is assumed as static. Since it is assumed that the initial heading is along the lane's direction, the values of θ could spread through the range of $[\beta, \pi/2 + \beta]$ and the initial $\omega^i{}_0$ is 0.

For the initialization of $q(t)$, in the straight road section, β is constant, while in the curved road section $\beta^i{}_0$ depends on [$x^i{}_0$, $y^i{}_0$]. $\beta^i{}_0$ is the corresponding angle within the local coordinates frame of the lane centre line. $d^i{}_0$ is the minimum distance between [$x^i{}_0$, $y^i{}_0$] and the lane central line.

The geometry relationship between the vehicle and lane is shown in Fig. 1.

where

X, Y, is local British National Grid coordinate system
X', Y', is vehicle body coordinate system
O, is the center of the vehicle

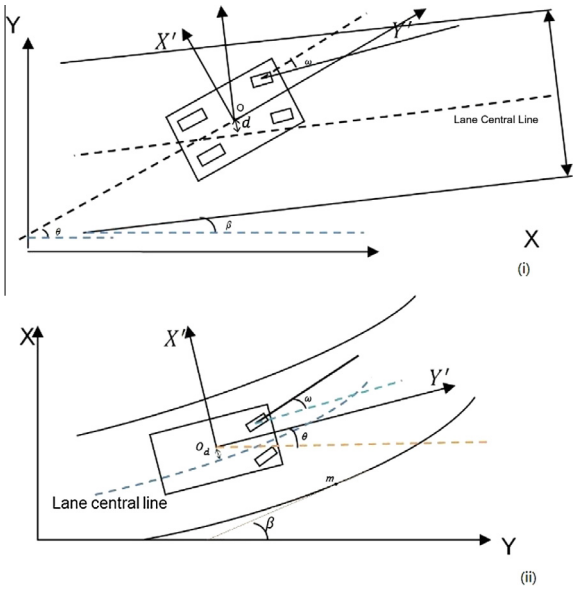

Fig. 1. Geometry relationship between vehicle and lane on a straight lane (i) and curved lane (ii).

θ, is the heading angle of the vehicle, which is also the angle between the vehicle body frame and the local British National Grid coordinate frame
ω, is the vehicle yaw rate
β, is the angle between the lane segment and the local British National Grid coordinates
d, is the vehicle lateral displacement, which is the distance between the O and lane central line

2.1.2. Filter prediction

The prediction model of the $p(t)$ is calculated as follows in Eq. (5):

$$(X) = \begin{pmatrix} x^i_{(t+1)} \\ y^i_{(t+1)} \\ v^i_{(t+1)} \\ \theta^i_{(t+1)} \\ \omega^i_{(t+1)} \\ a^i_{(t+1)} \end{pmatrix} = \begin{pmatrix} x^i_t \\ y^i_t \\ v^i_t \\ \theta^i_t \\ \omega^i_t \\ a^i_t \end{pmatrix} + \begin{pmatrix} \Delta^i_x \\ \Delta^i_y \\ \Delta^i_v \\ \Delta^i_\theta \\ \Delta^i_\omega \\ \Delta^i_a \end{pmatrix} \tag{5}$$

Δ^i_x, Δ^i_y, Δ^i_v , Δ^i_θ, $\Delta^i_\omega \Delta^i_a$ will be different from the vehicle motion models. In this paper, Constant Velocity (CV) and Constant Acceleration (CA) models are applied on straight highway motion, while Constant Turn Rate and Acceleration (CTRA) and Constant Turn Rate and Velocity (CTRV) models are applied on curved scenarios as they have perform a reasonable approx-imation of motions by vehicles on highways with straight and curves separately (Tsogas et al., 2005).

From the geometry relationship of the lane segment, the prediction of $q(t)$ can be expressed as:

$$\beta^i_{t+1} \approx \beta^i_t \tag{6}$$

$$d^i_{t+1} = d^i_t + \sin(\beta^i_t)\Delta^i_x - \cos(\beta^i_t)\Delta^i_y \tag{7}$$

2.1.3. Filter update

The prediction cycle is applied on every input sample. First, the judgment of d^i is made. The valid d^i should comply with the equation $|d^i| < 3HL$, where $3HL$ is 3 times half of the lane width. The reason for defining the threshold of parameter acceptance as $3HL$ is that it is not realistic for the vehicle jumps from current lane to the non-adjacent lane within 0.1 s based on the current lateral velocity. Assuming the lane width is 3.5 m, $3HL$ is 5.25 m. Thus, if $|d^i|$ is larger than 5.25 m, which means that the vehicle jumps from current lane to the non-adjacent lane. In that case, the particle is considered as measurement error (Toledo-Moreo et al., 2010).

If d^i is within this interval, the prediction parameters of $t + 1$ are calculated. However, these predictions are only considered as valid when the position predicted for a particle i is still within the bounds of the lane width. Therefore, after every prediction phase, the condition given by the following equation must be verified as below.

If $|d^i_{t+1}| < 3HL$ is satisfied and the predicted d^i_{t+1} is accepted, then the other predicted parameters are accepted. If $|d^i_{t+1}| < 3HL$ is not satisfied, the other predicted parameters are considered as invalid and the weighting of the particle is thus set as $w^i_0 = 0$. The weights of the samples are updated by the likelihood: $w^i_t = w^i_{t-1} p(Y_t|X^i_t) = w^i_{t-1} p_e(Y_t - h(X^i_t)), i = 1, 2, \ldots, N.$ where

X^i_t, is the parameter within the state vector (1) on the time epoch t with the particle number i.
Y_t, is the measurement for the parameters within the state vector (1) on the time epoch t.

GPS validity is tested after every prediction cycle and used to adjust the predicted particles to output the particle filter estimates.

2.1.4. Normalization and resampling

After every update phase, the weights of the particles are modified, and the normalization and resample test phases of a PF is relaunched.

2.2. Extended Kalman Filter model design

EKF is also an option for sensor fusion. The EKF is similar to the Kalman Filter (KF) but it can be applied on non-linear systems because it linearizes the transformations via the Taylor Expansion (Mohinder and Angus, 2008).

For the system developed in this paper, the EKF state vector, consisting of six parameters, is:

$$x(t) = (xy v \beta \theta \omega)^T \tag{8}$$

In this GPS/INS fusion system, the measurement space only includes four parameters of location, velocity and angle rate. The measurement vector is:

$$z(t) = (xy v \omega)^T \tag{9}$$

The relationship between measurement vector $z(t)$ and state vector $x(t)$ is:

$$z(t) = Hx(t) \tag{10}$$

The Jacobian of the measurement model H is:

$$H = \begin{pmatrix} 1 & 0 & 0 & 0 & 0 & 0 \\ 0 & 1 & 0 & 0 & 0 & 0 \\ 0 & 0 & 1 & 0 & 0 & 0 \\ 0 & 0 & 0 & 0 & 1 & 0 \end{pmatrix} \tag{11}$$

The covariance matrix of measurement noise is:

$$R = \begin{pmatrix} \sigma_x^2 & 0 & 0 & 0 \\ 0 & \sigma_y^2 & 0 & 0 \\ 0 & 0 & \sigma_v^2 & 0 \\ 0 & 0 & 0 & \sigma_\omega^2 \end{pmatrix} \tag{12}$$

The Jacobian of the measurement model with respect to measurement noise is:

$$V = \begin{pmatrix} \frac{\partial x}{\partial \sigma_x} & 0 & 0 & 0 \\ 0 & \frac{\partial y}{\partial \sigma_y} & 0 & 0 \\ 0 & 0 & \frac{\partial v}{\partial \sigma_v} & 0 \\ 0 & 0 & 0 & \frac{\partial \omega}{\partial \sigma_\omega} \end{pmatrix} \tag{13}$$

The estimated error covariance P is used together with the Jacobian matrix H and measurement noise covariance R together with the Jacobian matrix V to calculate the Kalman gain (Mohinder and Angus, 2008). Once the Kalman Gain K is calculated, the system brings in the measured data z to correct the predicted parameters and also the covariance error. After correcting the previously predicted values, the system is ready to predict the next position by using the state vector equations. The filter also estimates the error covariance of the estimated parameters by using the Jacobian of the system model with respect to state A and the Jacobian of the system model with respect to process noise W together with the process noise Q as follows.

$$A = \left[\frac{\partial y}{\partial x} f(x)\right] \tag{14}$$

$$W = \left[\frac{\partial y}{\partial w} f(x)\right] \tag{15}$$

Process noise covariance:

$$Q = \begin{pmatrix} w_x^2 & & & & & & \\ & w_y^2 & & & & & \\ & & w_{v_{cl}}^2 & & & & \\ & & & w_{\beta}^2 & & & \\ & & & & w_{\theta}^2 & & \\ & & & & & w_{\omega}^2 & \end{pmatrix} \tag{16}$$

For the four vehicle motion models (CV, CA, CTRV, CTRA), each one has its own EKF models. For every prediction, d is calculated to be the minimum distance between $[x, y]$ and the lane central line.

2.3. Simulation comparison of the positioning results

The simulation is created on the scenarios extracted from the true driving styles on straight and curved lanes. The most common irregular driving styles on straight lanes for highway are defined as weaving, swerving and jerky driving, while on the curved lane, weaving and jerky driving can occur, but swerving takes the form of over-turning or under-turning. Fig. 2 shows the defined different types of driving scenarios.

The simulation data generated by the GPS simulator and Matlab is used to feed the EKF and PF filters for the evaluation of the positioning results estimation. The details of the data generation is described in Sun et al. (2014). There are two filters

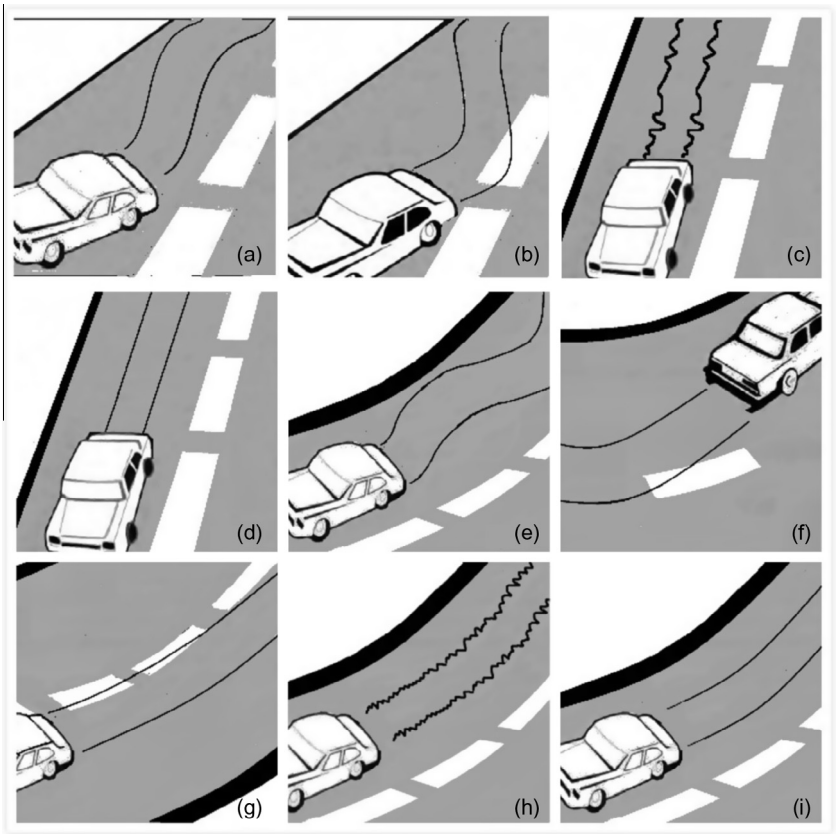

Fig. 2. Driving styles: (a) Scenario 1 weaving on straight. (b) Scenario 2 swerving on straight. (c) Scenario 3 jerky driving on straight. (d) Scenario 4 normal driving on straight. (e) Scenario 5 weaving on curve. (f) Scenario 6a swerving (over-turning) on curve. (g) Scenario 6b swerving (under-turning) on curve. (h) Scenario 7 jerky driving on curve. (i) Scenario 8 normal driving on curve (NHTSA, 2010).

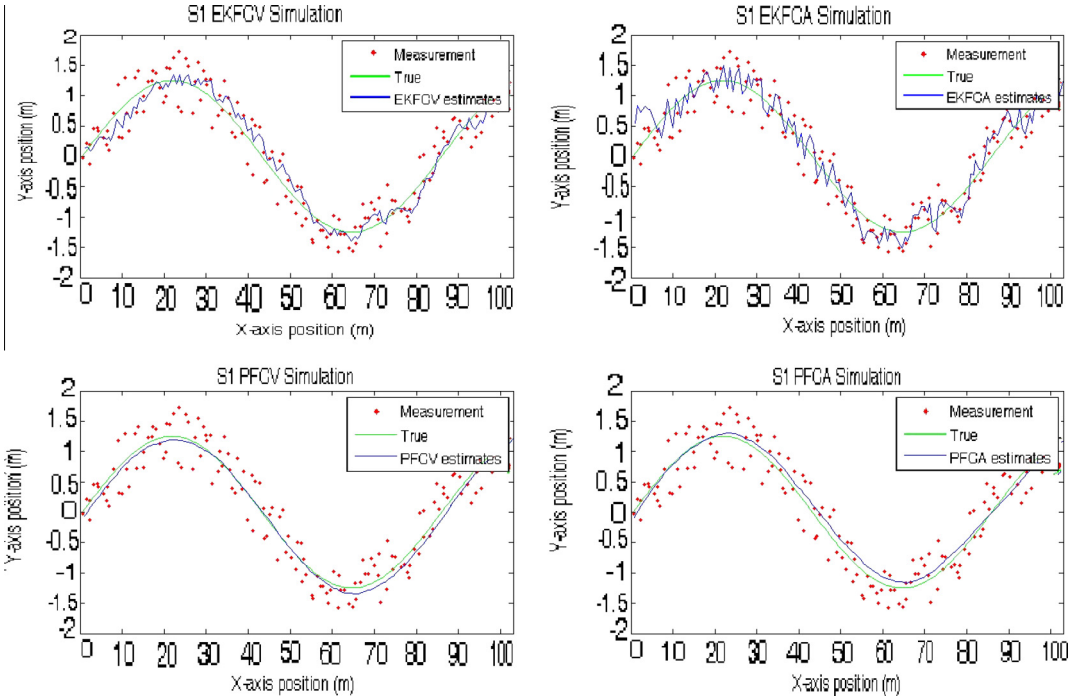

Fig. 3. Integrated estimation positioning results for Scenario 1.

Table 1
Mean positioning error results from model estimated results for straight scenarios.

Mean error comparison (m)	EKFCV/EKFCTRV	EKFCA/EKFCTRA	PFCV/PFCTRV	PFCA/PFCTRA
S1 weaving	0.3892	0.3873	0.2523	0.2032
S2 swerving	0.5521	0.5731	0.3363	0.3317
S3 jerky driving	0.5233	0.4910	0.3734	0.3676
S4 normal driving	0.6034	0.5873	0.4865	0.4731
S5 weaving on curve	0.5594	0.4487	0.4027	0.3888
S6a swerving (over-turning) on curve	0.5348	0.4658	0.3824	0.3696
S6b swerving (under-turning) on curve	0.4148	0.4012	0.3650	0.3581
S7 jerky driving on curve	0.7323	0.6720	0.5327	0.4231
S8 normal driving on curve	0.4547	0.4293	0.3870	0.3653

(EKF and PF) and four motion models (CV, CA, CTRV and CTRA), therefore, for the straight lane, the combination of fusion model can be EKFCV, EKFCA, PFCV and PFCA. For the curved lane, the combination of fusion model can be EKFCTRV, EKFCTRA, PFCTRV and PFCTRA.

By comparing of the integrated positioning results from EKFCV, EKFCA, PFCV and PFCA model estimations, in general, the EKF filters produce more noise, while the PF filter estimations are comparatively smooth, see Fig. 3 as an example for the integrated estimation positioning results for Scenario 1.

Vehicle mean positioning errors based on all designed model for straight and curved scenarios are shown in Table 1, which indicates that all of the fusion models have perform the positioning error below 1 m in all scenarios. Among these fusion models, PFCA/PFCTRA model performs the best estimation and makes the mean positioning error below 0.5 m in all of the scenarios, while the other models perform mean positioning error between 0.5 m and 1 m in some scenarios.

3. Irregular driving detection

The irregular driving features of the vehicle are extracted based on the defined scenarios. *Omega* and *d*, which are the vehicle's yaw rate and lateral displacement respectively, representing the vehicle's manoeuvres (Aljaafreh et al., 2012). In order to smooth the noises of the filter estimated values and extract the trend of their changes, Moving Average Deviation (MAD) of *omega* and *d*, noted as O-indicator and D-indicator respectively are developed to represent the driving features of the vehicle. The system to detect irregular driving has to recognize a driving event that characterizes the different driving styles on the FIS based irregular driving detection algorithms applied on O-indicator and D-indicator derived from the filter estimated *omega* and *d* at every time epoch.

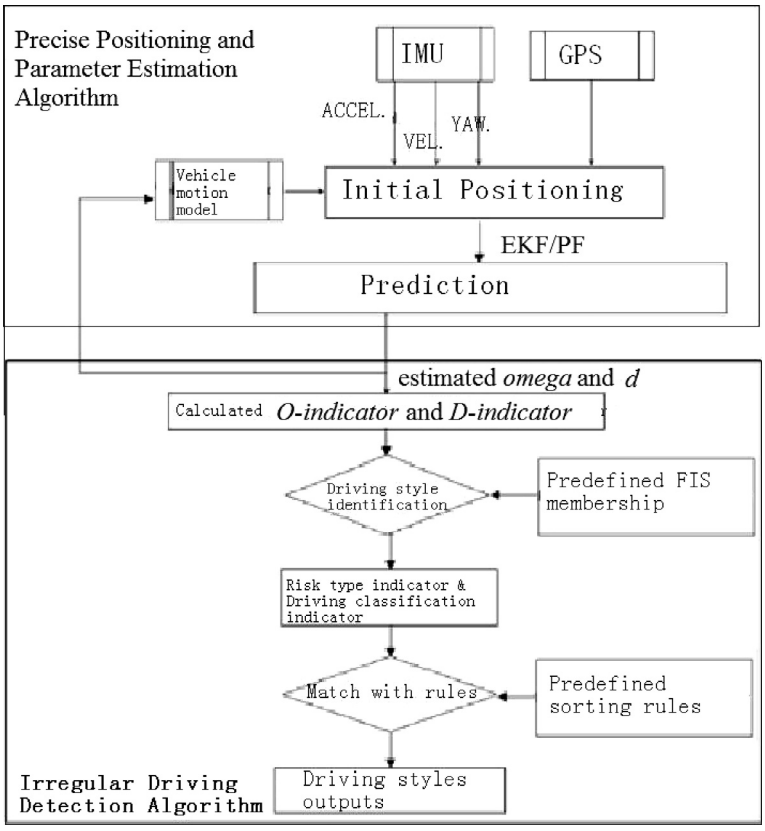

Fig. 4. Framework of the designed irregular driving detection system.

3.1. System overview

The Framework of the system in Fig. 4 shows the designed lane level irregular driving detection system, which contains two main parts. The first part is lane level precise positioning and parameter estimation algorithm. In order to collect the vehicle's driving data, one INS with one gyro and one accelerometer mounted along the vehicle body axis is used to output the yaw rate, acceleration and heading angle for the vehicle heading direction. One GPS is used to collect the vehicle's local coordinates and heading velocity. The collected initial position is used to feed the PF/EKF models with the precise vehicle motion models to provide the estimated positioning and attitude parameters for the next time epoch for iteration. This part has already discussed in Section 2. The second part is irregular driving detection algorithm. It started from the calculation of O-indicator and D-indicator based on the first part estimated *omega* and *d*. These two indicators are then as the input of the FIS for the driving pattern identification. The FIS outputs the risk type indicator. In order to amplify the features of each driving style, the driving classification indicators are then developed based on the risk type indicators. Finally, by comparison of the sorting of calculated driving classification indicator with predefined sorting rules extracted from the reference data, the system will output the identified driving style type.

3.2. FIS based detection algorithm

For each designed irregular driving style, the different sorting of the driving classification indicator can present different driving styles. In order to pick up the features, the FIS is applied on the O-indicator and D-indicator to output the risk type indicator.

The FIS is a widely used pattern matching method for detecting driver behaviour. It maps input to output using fuzzy logic through combination rules. The membership function of a fuzzy set is a generalization of the indicator function in classical sets. In FIS, it represents the degree of truth as an extension of evaluation (Zadeh, 1965). The fuzzy inference system consists of three stages. The first stage is fuzzification, which maps any input to a degree of membership in one or more membership functions and the input variable is evaluated in terms of the linguistic condition. The second stage is fuzzy inference, which calculates the fuzzy output. The final step is defuzzification, which is to convert the fuzzy output to a crisp output (Aljaafreh et al., 2012).

Based on the output of the risk type indicator values for every time epoch, the total risk type indicator numbers in defined risk types are calculated followed by driving classification indicator. The sorting rules extracted from driving classification indicators of the reference data is applied to the integrated model estimated driving classification indicator data to judge the driving types.

The O-indicator and D-indicator estimated from the fusion model are the input of the FIS system to calculate the risk type indicator for each fusion model. Fig. 5 shows the structure of the fuzzy inference system.

Figs. 6 and 7 show the designed membership function for the O-indicator and D-indicator values and risk type indicator in straight and curved scenarios. The experience data is used to define the fuzzy values in the membership functions. In Figs. 6 and 7, O-indicator is the first input of FIS and corresponding fuzzy values are defined to be Small O-indicator (SO), Medium O-indicator (MO), Large O-indicator (LO) and Very Large O-indicator (VLO). The trapezoidal membership function is used for the SO and VLO fuzzy sets and the triangular function is used for MO and BO. D-indicator is the second input of FIS and the corresponding fuzzy values are defined to be Small D-indicator (SD), Medium D-indicator (MD), Large D-indicator (LD) and Very Large D-indicator (VLD). The trapezoidal membership function is used for the SD and VLD fuzzy sets and the triangular function is used for MD and BD. Finally, the system output driving risk type indicator, defined by four fuzzy values A, B, C, D. Fuzzy value A means low risk, B means medium risk, C means high risk and D means very high risk. Trapezoidal membership function is used for A and D fuzzy sets and the triangular function is used for the B and C fuzzy sets.

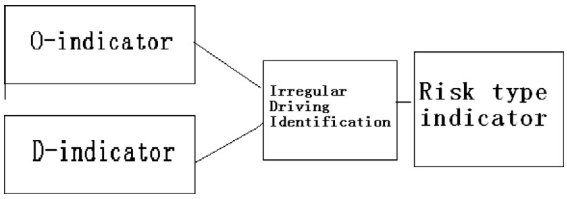

Fig. 5. Fuzzy inference system structure.

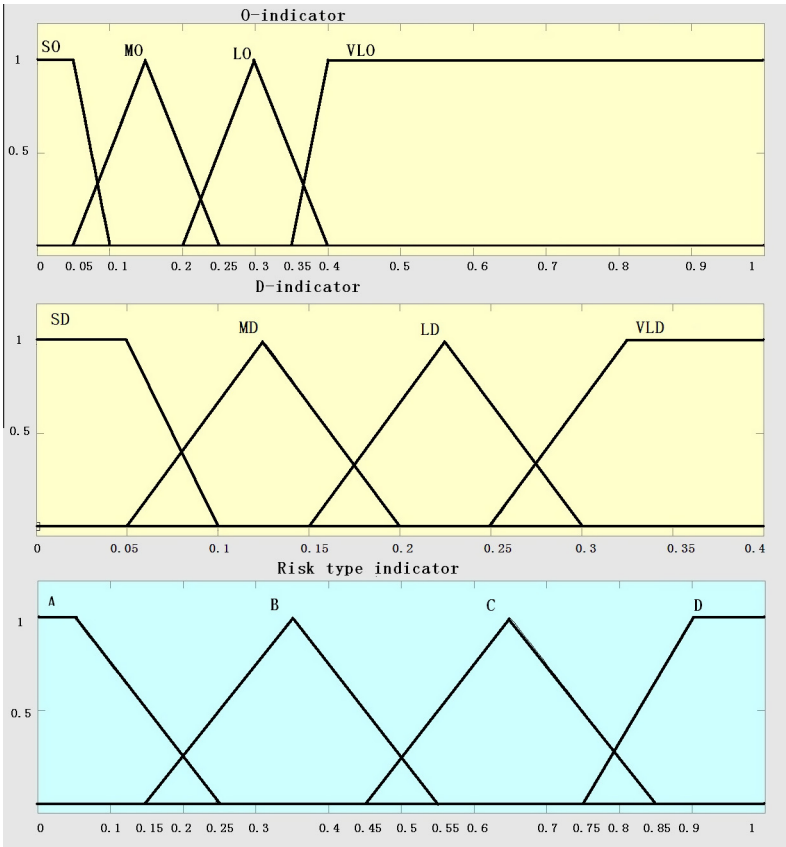

Fig. 6. Membership function for the straight scenarios.

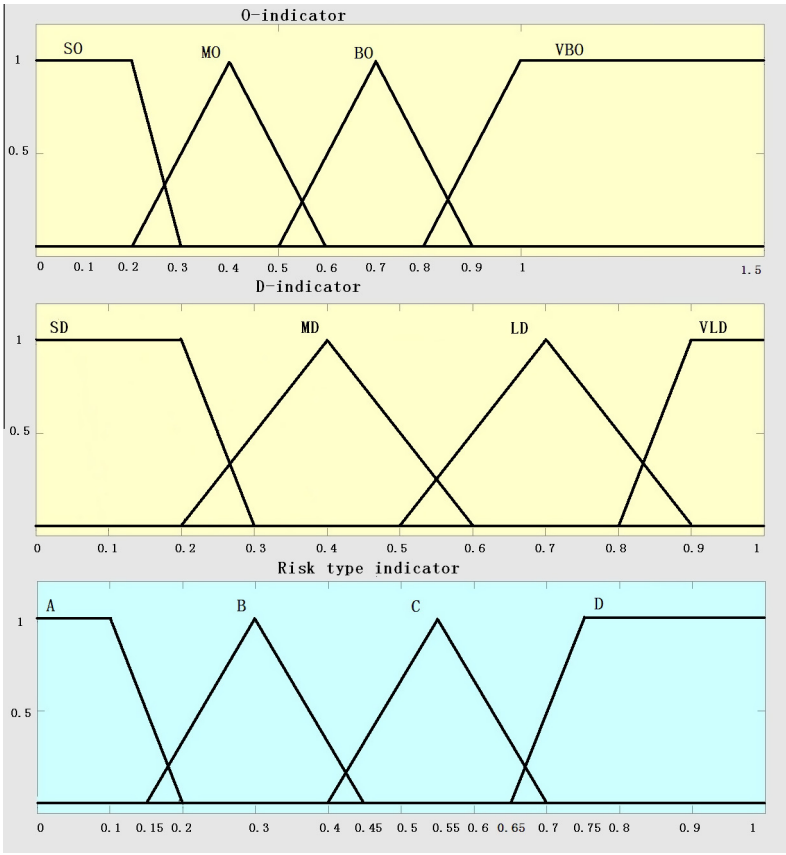

Fig. 7. Membership function for the curved scenarios.

Table 2
Rules of FIS for straight scenarios.

O-indicator	D-indicator	Risk type
SO	SD	A
	MD	B
	LD	C
	VLD	
MO	Any(SD, MD, LD,VLD)	C
LO	Any(SD, MD, LD,VLD)	D
VLO	Any(SD, MD, LD,VLD)	D

The rules for mapping the O-indicator and D-indicator to the corresponding risk type is based on the experience data. Tables 2 and 3 show the mapping rules for straight and curved scenarios. Fig. 8 shows the designed FIS results in surface view, which presents the one pair of O-indicator value and D-indicator value has one corresponding risk type indicator value.

Based on the risk type indicator output of the FIS, the points in each risk type for all the scenarios during the last 5 s are collected and calculated in Simulink. Table 4 shows the statistics of the number of points in each risk type calculated from the reference data. It can be seen that each scenario returns one or two dominant risk types in the 5 s sample. If there was only one dominant risk type for a given scenario containing the most points, it would be straightforward to classify the scenarios. However, this is not always the case with two or more risk types having a similar number of points for some scenarios. In order to amplify the features of each scenario, the points in adjacent risk types are combined as shown in Table 5, effectively resulting in new driving classification indicator for the detection of driving styles. The four parameters in driving classification indicator are developed based on the sum number of points in adjacent risk types, e.g., AB is the sum number of risk type A and risk type B; BC is the sum number of risk type B and risk type C; CD is the sum number of risk type C and risk type D; AD is the sum number of risk type A and D.

Table 3
Rules of FIS for curved scenarios.

O-indicator	D-indicator	Risk type
SO	SD	A
	MD	B
	LD	D
	VLD	
MO	SD	B
	MD	
	LD	D
	VLD	
LO	SD	C
	MD	
	LD	
	VLD	D
VLO	SD	C
	MD	
	LD	
	VLD	D

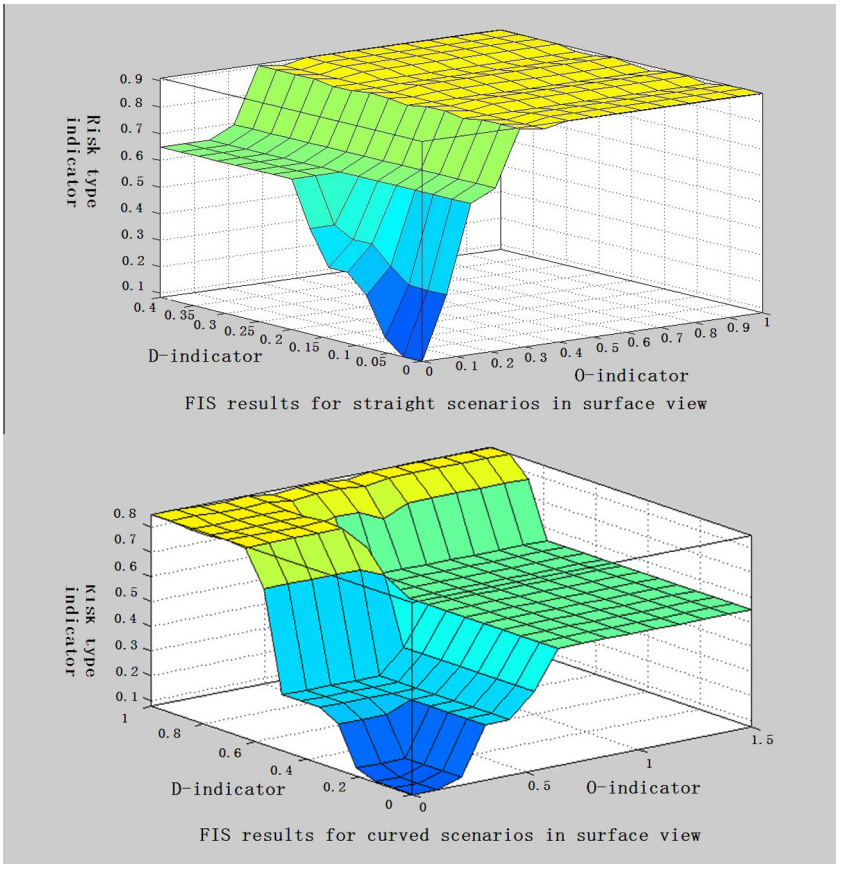

Fig. 8. Designed FIS logic in surface view.

Based on the calculation and comparison results of the AB, BC, CD and AD parameters, the sorting rules can be extracted to represent the feature of each scenario. For example, AB > BC > CD > AD is extracted as the rule for weaving from S1 and CD > BC = AD > AB is extracted from S7 as jerky driving. Thus, the rules for detecting the features of each of the scenarios are extracted in Table 6. Based on the sorting rules extracted, the simulated reference episode is generated to test the performance of the irregular driving detection algorithm in Section 3.3.

Table 4
Statistic of number of points in risk types indicators for reference data.

Number of points	Risk types			
Scenarios	A	B	C	D
S1	19	31	0	0
S2	15	11	22	2
S3	0	1	11	38
S4	50	0	0	0
S5	8	40	2	0
S6a	0	25	19	6
S6b	10	28	12	0
S7	0	3	22	25
S8	50	0	0	0

Table 5
Driving classification indicators for reference data.

Scenarios	AB	BC	CD	AD
S1	50	31	0	19
S2	26	33	24	17
S3	1	12	49	38
S4	50	0	0	0
S5	48	42	2	8
S6a	25	44	25	6
S6b	38	40	12	10
S7	3	25	47	25
S8	50	0	0	50

Table 6
Sorting rules for driving style judgment.

No.	Sorting rules	Judgment
1	AB > BC >= CD >= AD	Weaving/weaving on curve
2	AB > BC >= AD >= CD	Weaving/weaving on curve
3	AB > CD >= BC >= AD	N/A
4	AB > CD >= AD >= BC	Weaving/weaving on curve
5	AB > AD >= BC >= CD	Normal driving/normal driving on curve
6	AB > AD >= CD >= BC	N/A
7	BC > CD >= AD >= AB	Swerving/over-turning (under-turning)
8	BC > CD >= AB >= AD	Swerving/over-turning (under-turning)
9	BC > AD >= AB >= CD	N/A
10	BC > AD >= CD >= AB	N/A
11	BC > AB >= CD >= AD	Swerving/over-turning (under-turning)
12	BC > AB >= AD >= CD	Swerving/over-turning (under-turning)
13	CD > AD >= AB >= BC	Jerky driving/jerky driving on curve
14	CD > AD >= BC >= AB	Jerky driving/jerky driving on curve
15	CD > AB >= BC >= AD	N/A
16	CD > AB >= AD >= BC	N/A
17	CD > BC >= AB >= AD	N/A
18	CD > BC >= AD >= AB	Jerky driving/jerky driving on curve
19	AD >= AB >= BC >= CD	Normal driving/normal driving on curve
20	AD > AB >= CD >= BC	Normal driving/normal driving on curve
21	AD > CD >= AB >= BC	Jerky driving/jerky driving on curve
22	AD > CD >= BC >= AB	Jerky driving/jerky driving on curve
23	AD > BC >= AB >= AD	N/A
24	AD > BC >= AD >= AB	N/A
25	AB = AD	Normal driving/normal driving on curve

3.3. Simulated reference trajectory for the irregular driving detection

The simulated reference episode of irregular driving types are input for the test to find out if the irregular driving detection algorithm can continuously detect different types of irregular driving. One set of 60 s episode is created to test the irregular driving detection algorithm. Fig. 9 shows the trajectory of the designed episode. The simulated data includes the manoeuvres with weaving for 10 s, swerving for 10 s, jerky driving for 10 s and normal driving for 30 s. The separate irregular driving manoeuvre for the episode test has already been recognized in the previous paper (Sun et al., 2014).

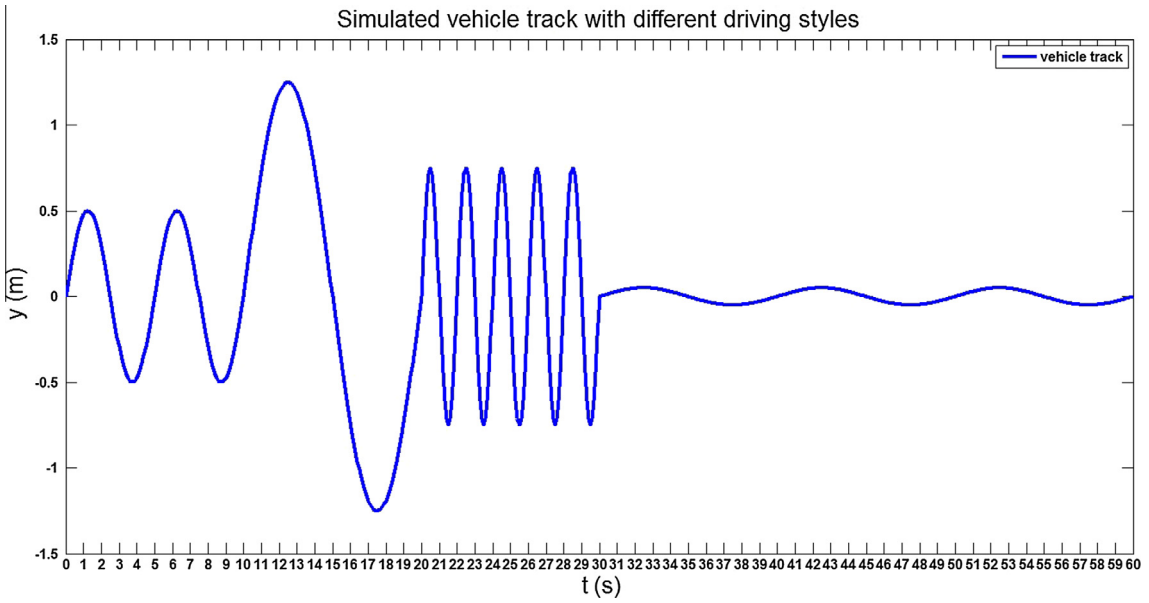

Fig. 9. Input episode with different driving styles.

Table 7
Detection results for the episode.

Output frequency (Hz)	First detection time epoch			
	Weaving	Swerving	Jerky driving	Normal driving
10	5 s	14.5 s	21.8 s	32.7 s
5	5 s	14.5 s	22 s	33 s
1	5 s	15 s	22 s	33 s

The irregular driving detection results for the episode test are output in 10 Hz, 5 Hz and 1 Hz, see Table 7.

Table 7 reveals several information of the irregular driving detection results for the episode. As the algorithm use back 5 s data to judge the irregular driving styles, the first irregular driving detection result output time epoch is in the 5 s. From the comparison of the irregular driving detection output in different frequencies, it is shown that if the output frequency is higher, the detection of the specific irregular driving can be earlier. For example, if the output frequency is 5 Hz, the first time to detect jerky driving is in the time epoch 22 s, however, if the frequency is 10 Hz, the first time to detect jerky driving could be 21.8 s, which is 0.2 s earlier than using 5 Hz output.

Availability and correct detection rate are parameters developed to evaluate the performance of the irregular driving detection algorithm. Availability is the percentage of the available driving style detection output. Correct detection rate is the percentage of the correct driving style judgement output. In general, although the episode test results show that every designed irregular driving styles can be distinguished and detected, there are still some problems exit in the detection of irregular driving. Fig. 10 is an example of the unavailability in the detection of the irregular styles in 5 Hz output rate. The driving classification indicator in the blue block forms the sorting rule CD = AD > AB = BC, which cannot output any driving styles. These kind of unavailability always happen in the changing area from one driving style to another. The availability and correct detection rate for the episode is shown in Table 8 and it is clear that if the output rate of the system is higher, the correct detection rate and availability rate will decrease. Thus, choose the proper output rate for required situation is critical.

3.4. Fusion model estimated results for irregular driving detection

From the fusion model estimated results based irregular driving detection in the simulation, the performance is discussed based on the positioning error levels. The models with the mean positioning estimation errors above 0.5 m are EKFCV, EKFCTRV, EKFCA, EKFCRA and PFCTRV. EKFCV and EKFCTRV results have wrongly detected swerving/under-turning as jerky driving or weaving. EKFCA and EKFCTRA models results both have wrongly detected weaving/weaving on curve as swerving/swerving on curve. Furthermore, EKFCTRA results also have wrongly detected normal driving as weaving on curve. PFCTRV model results incorrectly detect swerving on curve as weaving on curve. It is obviously that none of the model estimations results above can be used for the correct detection of the irregular driving scenarios, resulting from the low positioning accuracy. PFCV, PFCA and PFCTRA models have the mean positioning estimation error below 0.5 m. All three models based

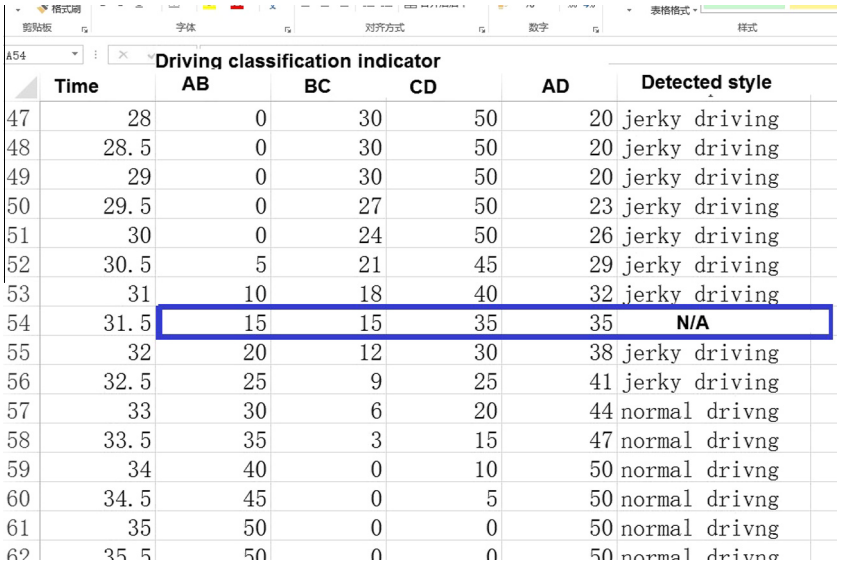

	Time	AB	BC	CD	AD	Detected style
47	28	0	30	50	20	jerky driving
48	28. 5	0	30	50	20	jerky driving
49	29	0	30	50	20	jerky driving
50	29. 5	0	27	50	23	jerky driving
51	30	0	24	50	26	jerky driving
52	30. 5	5	21	45	29	jerky driving
53	31	10	18	40	32	jerky driving
54	31. 5	15	15	35	35	N/A
55	32	20	12	30	38	jerky driving
56	32. 5	25	9	25	41	jerky driving
57	33	30	6	20	44	normal drivng
58	33. 5	35	3	15	47	normal drivng
59	34	40	0	10	50	normal drivng
60	34. 5	45	0	5	50	normal drivng
61	35	50	0	0	50	normal drivng
62	35. 5	50	0	0	50	normal drivng

Fig. 10. An example of unavailability in detection of irregular driving.

Table 8
The availability and correct detection rate for the episode analysis with respect to output rate.

Output rate (s)	Availability (%)	Correct detection rate (%)
0.1	94.19	97.82
0.5	98.19	98.20
1	98.21	100

estimations have correctly detected different irregular driving scenarios. Thus, from the simulation, it can be concluded that 0.5 m mean positioning accuracy is required for the irregular driving detection algorithm.

In the next section, the field test is carried out to validate the designed lane level high accuracy positioning based irregular driving detection algorithm. The PFCA and PFCTRA model perform the best positioning estimations in the simulation will be applied on the true GPS data collected on the highway.

4. Field experiment and analysis

The field test is based on the real time single reference Real Time Kinematic (RTK) GPS data filtered with PFCTRA and PFCA estimation to input into the FIS for detection of irregular driving. The road test includes the design of the data collection scheme and its execution including the analysis of the results of the detection of irregular driving.

4.1. Data collection

The designed driving routes for the experiment are on the M4 highway from Ravenscourt Park to Heathrow Terminal 3 and then back to Imperial College London. The irregular driving styles are conducted on the two routes captured. For the first route in the east–west direction, data were captured for 7 min, involving weaving and jerky driving on a straight lane and jerky driving on a curved lane. For the second route in the west–east direction, data were captured for 3 min, involving swerving and weaving on a curved lane. Therefore, in order to distinguish different types of irregular driving, total five sessions are defined in Table 9. All the sessions are carried out on the open area when there was no passing by vehicle or trees on the highway, that is to ensure the safety of the experiment and also the relatively high quality RTK measurements obtained from the GPS. As the experimental vehicle is old and potentially dangerous for some types of manoeuvres, swerving was attempted only once.

For the irregular driving data collection, the vehicle was driven at speeds ranging from 70 km/h to 120 km/h and the data is collected at 10 Hz. The installation of the various equipment is shown in Fig. 11. The specifics of the equipment used in the experiment were as follows.

Table 9
Definition of sessions.

Session name	Start time (UTC)	End time (UTC)	Driving type
Session 1	15:51:14.0	15:51:20.8	Weaving on straight
Session 2	15:51:41.5	15:51:50.4	Jerky driving on curve
Session 3	15:57:13.9	15:57:23.5	Jerky driving on straight
Session 4	16:12:10.9	16:12:16.1	Swerving on curve
Session 5	16:12:36.4	16:12:43.4	Weaving on curve

Fig. 11. On board equipment.

- Leica Viva GNSS GS15 receiver for real-time GPS data collection, including the position and speed of the vehicle.
- I-Mar RT-200 INS for the real-time attitude data collection, including heading angle and yaw rate of the vehicle. The sensor have the function of output GPS/INS measurements, which were post-processed by forward and backward processing using Inertial Explorer for a high accuracy reference.

For the collected irregular driving styles, the post-process GPS/INS measurements are directly feed to irregular driving detection algorithm to make the reference. The measurements output from Leica Viva GNSS GS15 is to feed the PFCA/PFCTRA model for positioning and dynamic parameter estimation and then the estimated results are used for irregular driving detection algorithm.

Besides the collection of irregular driving trajectory data, another important issue is to get the lane's central line data in the field test. In this thesis, the coordinates information of lane's central line is collected afterwards by the vehicle with i-Mar RT-200 INS (20 Hz output rate) driving along the middle of the lanes, on which the irregular driving are conducted. The post-processed GPS/INS measurements for the central line are recognized as the lane's central line coordinates information. The lateral displacement of the vehicle will be calculated by the same method as in simulation, which is searching for the nearest two points of the central line data to the vehicle's location and then calculate the perpendicular distance to the straight line containing these two points. Therefore, the calculated perpendicular distance is the lateral displacement of the vehicle.

4.2. Reference data for irregular driving detection

The post-processed data collected by the high-grade integrated system on the routes are considered as the reference data in the field test. For the defined sessions, the calculated O-indicator and D-indicator from the reference data are feed to the FIS model to output the risk type indicator values and driving classification indicator values in three output rates (1 Hz, 5 Hz and 10 Hz) for both routes. The example of the calculated driving classification indicator values from the reference data for the first 5 s is in Table 10. It shows that the irregular driving is correctly detected in the first five seconds sample.

Table 10
Driving classification indicators for the first five seconds of five sessions from reference data.

Sessions	Five seconds of sessions	AB	BC	CD	AD	Judgement
1	15:51:14.0–15:51:18.9	47	44	3	6	Weaving on straight
2	15:51:41.5–15:51:46.4	0	31	50	19	Jerky driving on curve
3	15:57:13.9–15:57:18.8	0	9	50	41	Jerky driving on straight
4	16:12:10.9–16:12:15.8	29	31	21	19	Swerving on curve
5	16:12:36.4–16:12:41.3	50	41	0	9	Weaving on curve

Table 11
The first time epoch of irregular driving detection for sessions based on the output frequency from reference results.

Output frequency (Hz)	First detection time epoch				
	Session 1	Session 2	Session 3	Session 4	Session 5
10	15:51:16.2	15:51:45.8	15:57:15.3	16:12:14.5	16:12:39.7
5	15:51:16.5	15:51:46.0	15:57:15.5	16:12:14.5	16:12:40.0
1	15:51:17.0	15:51:46.0	15:57:16.0	16:12:15.0	16:12:40.0

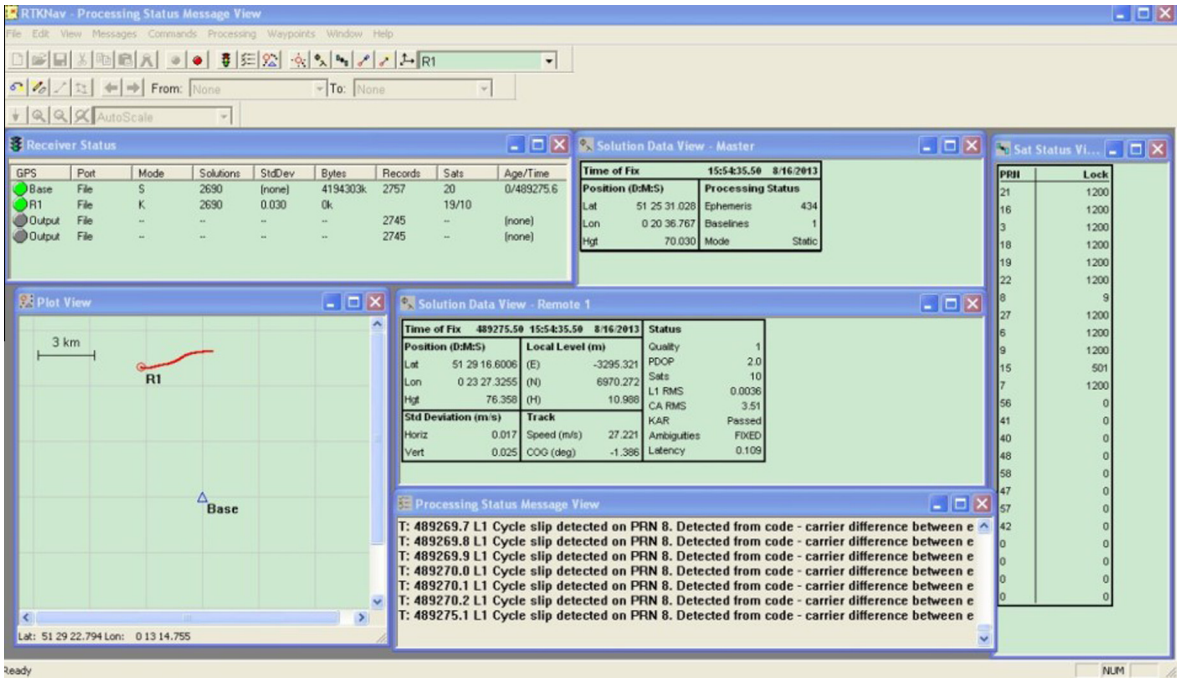

Fig. 12. RTKNav processing.

The first detection time epoch of different types of irregular driving based on the various output rate is shown in Table 11. It is clear that all of the sessions can be detected within the five seconds of the irregular driving happen. The reference data based field test results show the irregular driving detection can be detected on the routes. It also indicates that the higher output rate, the earlier detection time epoch, which is identical with the simulation results.

From the post-processed GPS/INS combined reference data based irregular driving detection results, it is clear that the defined irregular driving styles can be distinguished on a highway. In Section 4.3, the RTK GPS measurements with PFCA and PFCTRA models used for the detection of irregular driving detection will be discussed.

4.3. Fusion results for irregular driving detection

The NovAtel RTKNav software has been used to process the collected Leica GPS receiver data. The output contains the position and velocity of the vehicle at each time epoch at 10 Hz. The quality of positioning was measured in 4 types: type 0 for no solution, type 1 for single point positioning, type 2 for DGPS positioning, type 3 for PPS DGPS positioning, type 4 for RTK ambiguity fixed positioning and type 5 for RTK float ambiguity solution. Fig. 12 shows the reply mode based real-time simulation processing for the collected data in RTKNav software. The reply mode can simulate the real situation with the same time duration.

From the RTKNav output for the positioning quality solutions. 84.04% of total points were determined with the RTK fixed ambiguity solution in route 1, which is claimed to have sub-meter mean positioning accuracy. However, in route 2, only 51.53% of the points were determined with the RTK fixed ambiguity solution. As it is discussed in the simulation, 0.5 m positioning accuracy is required for the irregular driving detection, current RTKNav output positioning is obviously not accuracy enough. For this reason, the PFCA and PFCTRA models have shown the smallest errors in the straight and curved positioning estimation in the simulation is used for the real sessions to improve RTK GPS positioning accuracy.

From Fig. 13, it is clear that the filter estimated results are closer to the reference position solutions, demonstrating benefit of filtering to the improvement of the accuracy of the RTK GPS results. Table 12 shows the statistics of the positioning

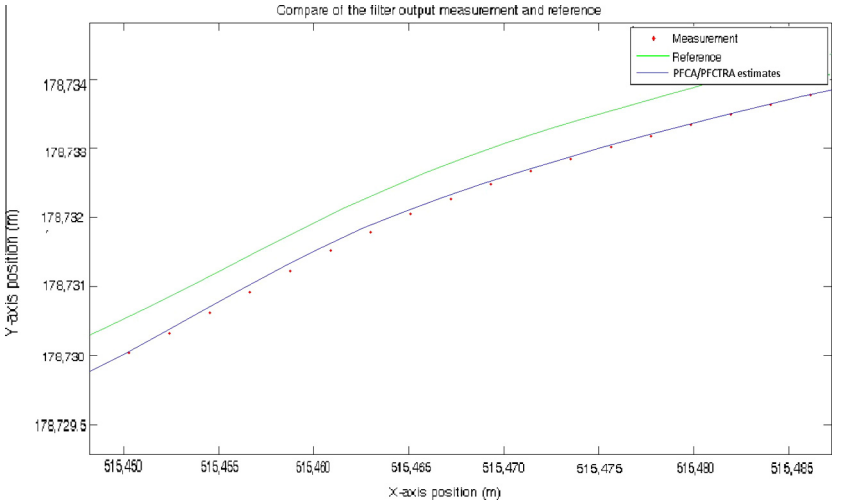

Fig. 13. Comparison of RTKNav output GPS positioning and PFCA/PFCTRA estimated positioning results with respect to reference.

Table 12
Statistics of the positioning accuracy.

Name	Time	Positioning type	Error in 0–0.5 m	Error in 0.5–1 m	Error in 1–1.5 m	Error Above 1.5 m	Total
Route 1	15:51:00–15:57:59.9	RTKNav output points	48	1498	2633	20	4199
		PFCA/PFCTRA estimated points	305	3455	422	17	4199
		RTKNav output Percentage	1.14%	35.68%	62.70%	0.48%	100%
		RTKNav output mean error	0.9664 (m)				
		PFCA/PFCTRA estimated percentage	7.26%	82.28%	10.06%	0.40%	100%
		PFCA/PFCTRA estimated mean error	0.6214 (m)				
Route 2	16:10:00–16:12:59.9	RTKNav output points	96	481	1179	43	1799
		PFCA/PFCTRA estimated points	375	1116	277	31	1799
		RTKNav output Percentage	5.33%	26.72%	65.56%	2.39%	100%
		RTKNav output mean error	1.0090 (m)				
		PFCA/PFCTRA estimated percentage	20.84%	62.03%	15.41%	1.72%	100%
		PFCA/PFCTRA estimated mean error	0.7883 (m)				

performance for route 1 and route 2. It is obviously that PFCA/PFCTRA model estimated positioning solutions have significantly improved the positioning accuracy compared to RTKNav output results, which indicate that the mean positioning error in route 1 is reduced to 0.6214 m from 0.9664 m and the mean positioning error in route 2 is reduced to 0.7883 m from 1.0090 m. The percentage of measurements positioning errors within 0–0.5 m in route 1 is increased from 1.14% to 7.26% based on the PFCA/EKFCTRA estimations, meanwhile, the corresponding percentage for route 2 is increased from 5.33% to 20.84%. Furthermore, from the analysis of positioning accuracy against the time epochs of the defined sessions, it shows that the mean positioning error after PFCA/PFCTRA model applied for all the 5 sessions are below 0.5 m.

Based on the PFCA/PFCTRA estimated positioning results, the 5 s example of driving classification indicator and judgement from the PFCA/PFCTRA estimated results are presented in Table 13. In the example of the first five seconds of the five sessions, the detection of different types of irregular driving results are identical with the reference data based irregular driving detection results.

The first time epoch for detection of irregular driving manoeuvres based on the PFCA/PFCTRA estimated results in Table 14 performs similar results with the reference data, which means that the PFCA/PFCTRA estimated results are capable of distinguishing defined sessions. The comparison of the availability and correct detection rate of the irregular driving detection algorithm with respect to the output rate is shown in Table 15. Generally, the availability and correct detection rate of the irregular driving detection algorithm decrease as the output rate increase. The availability based on the PFCA/PFCTRA estimated results is slightly lower than the availability from the reference results. The correct detection rate from PFCA/PFCTRA estimations is significantly lower than the reference, as the PFCA/PFCTRA estimations have more error than the reference.

From the analysis of the sessions above, the 0.5 m positioning accuracy requirement for the irregular driving detection algorithm is validated in the field test. However, there are a number of open issues associated with real testing. Due to low quality satellite signal especially during the time interval just after crossing an over-bridge, the collected trajectory data on the initial time for recapture of the signal is a bit fluctuate. Similar situation also occurs as a result of vehicle passing by

Table 13
The example of driving classification indicator for the first five seconds of five sessions from PFCA/PFCTRA estimated data.

Session	AB	BC	CD	AD	Judgement
1	49	46	1	4	Weaving on straight
2	0	27	49	23	Jerky driving on curve
3	0	5	50	45	Jerky driving on straight
4	27	31	25	20	Swerving on curve
5	48	44	2	6	Weaving on curve

Table 14
The first time epoch of irregular driving detection for sessions based on the output frequency from PFCA/PFCTRA estimated results.

Output frequency (Hz)	First detection time epoch				
	Session 1	Session 2	Session 3	Session 4	Session 5
10	15:51:16.4	15:51:45.9	15:57:15.3	16:12:14.8	16:12:39.6
5	15:51:16.5	15:51:46.0	15:57:15.5	16:12:15.0	16:12:40.0
1	15:51:17.0	15:51:46.0	15:57:16.0	16:12:15.0	16:12:40.0

Table 15
The comparison of availability and correct detection rate from the PFCA/PFCTRA estimated results and reference results with respect to different output rates.

Output rate (s)	Availability (PFCA/PFCTRA estimated) (%)	Availability (reference) (%)	Correct detection rate (PFCA/PFCTRA estimated) (%)	Correct detection rate (reference) (%)
0.1	86.13	87.12	79.82	87.35
0.5	92.35	93.27	89.20	94.05
1	94.21	95.34	94.71	96.75

proximate objects such as large lorries and trees. These problems results from the GPS signal weakness, although the PFCA/PFCTRA estimated GPS positioning improves accuracy, however, due to the low quality measurement data, it is still impossible to make all of the measurement positioning accuracy below 0.5 m, which is the positioning accuracy requirement for the irregular driving detection algorithm. That is also the reason why the correct detection rate for the PFCA/PFCTRA estimation based irregular driving detection algorithm is much lower than the reference especially in high rate output mode. For the future work, the Trimble BD910 receiver module, which is claimed to be capable of providing centimeter moving positioning accuracy, may be used to evaluate if the positioning results and irregular driving detection performance could be improved.

5. Conclusion

This paper presents a novel integrated solution for lane level irregular driving detection on the highways. The PFCA/PFCTRA evaluated as the best performance fusion model for GNSS/INS integration during the simulation is further verified in the real road test, the results show that the developed PFCA and PFCTRA model have improved the accuracy of the RTK GPS measurements and based on the 0.5 m positioning accuracy, the defined weaving, swerving and jerky driving sessions can be detected correctly on the highway.

References

Albu, A.B., Widsten, B., Wang, T., Lan, J., Mah, I., 2008. A computer vision-based system for real-time detection of sleep onset in fatigued drivers. In: 2008 IEEE Intelligent Vehicles Symposium, pp. 25–30.

Aljaafreh, A., 2012. Web driving performance monitoring system. World Academy of Science, Engineering and Technology 70, 2012.

Aljaafreh, A., Alshabatat, N., Najim Al-Din, M.S., 2012. Driving style recognition using fuzzy logic. In: 2012 IEEE International Conference on Vehicular Electronics and Safety (ICVES), pp. 460–463.

Chang, T.H., Hsu, C.S., Wang, C., Yang, L.K., 2008. Onboard measurement and warning module for irregular vehicle behavior. IEEE Trans. Intell. Transp. Syst. 9 (3), 501–513.

Dai, J., Teng, J., Bai, X., Shen, Z., Xuan, D., 2010. Mobile phone based drunk driving detection. In: 2010 4th International Conference on Pervasive Computing Technologies for Healthcare (Pervasive Health), pp. 1.

Desai, A.V., Haque, M.A., 2006. Vigilance monitoring for operator safety: a simulation study on highway driving. J. Saf. Res. 37 (2), 139–147.

Eriksson, M., Papanikolopoulos, N.P., 2001. Driver fatigue: a vision-based approach to automatic diagnosis. Transp. Res. Part C: Emerg. Technol. 9 (6), 399–413.

Gustafsson, F., Gunnarsson, F., Bergman, N., Forssell, U., Jansson, J., Karlsson, R., Nordlund, P.-J., 2002. Particle filters for positioning, navigation and tracking. IEEE Trans. Signal Process. 50, 425–435.

Heitmann, A., Cuttkuhn, R., Aguirre, A., Trutschel, U., Moore-Ede, M., 2001. Technologies for the monitoring and prevention of driver fatigue. In: Proceedings of the Fifth International Driving Symposium on Human Factors in Driver Assessment, Training and Vehicle Design, pp. 81–86.

Imkamon, T., Saensom, P., Tangamchit, P., Pongpaibool, P., 2008. Detection of hazardous driving behavior using fuzzy logic. In: 5th International Conference on Electrical Engineering/Electronics, Computer, Telecommunications and Information Technology, ECTI-CON 2008. 2, pp. 657.
Kilbey, P., 2013. Reported Road Casualties in Great Britain: 2012 Annual Report. Department of Transport.
Krajewski, J., Sommer, D., Trutschel, U., Edwards, D., Golz, M., 2009. Steering wheel behavior based estimation of fatigue. In: Proceedings of the Fifth International Driving Symposium on Human Factors in Driver Assessment, Training and Vehicle Design, pp. 118–124.
Lecce, V.D., Calabrese, M., 2008. Experimental system to support real time driving pattern recognition. Advanced Intelligent Computing Theories and Applications with Aspects of Artificial Intelligence Annals of Emergency Medicine, pp. 1192–1199.
Lee, J.D., Li, J.D., Liu, L.C., Chen, C.M., 2006. A novel driving pattern recognition and status monitoring system. In: Chang, L.-W., Lie, W.-N. (Eds.), Advances in Image and Video Technology, ser. Lecture Notes in Computer Science, vol. 4319. Springer, Berlin/Heidelberg, pp. 504–512.
Mohinder, S.G., Angus, P.A., 2008. Kalman Filtering: Theory and Practice Using MATLAB. Wiley-IEEE Press.
NHTSA, 2010. <http://www.nhtsa.gov/>.
Omidyeganeh, M., Javadtalab, A., Shirmohammadi, S., 2011. Intelligent driver drowsiness detection through fusion of yawning and eye closure. In: 2011 IEEE International Conference on Virtual Environments Human–Computer Interfaces and Measurement Systems (VECIMS), pp. 1–6.
Sandberg, D., Akerstedt, T., Anund, A., Kecklund, G., Wahde, M., 2011. Detecting driver sleepiness using optimized nonlinear combinations of sleepiness indicators. IEEE Trans. Intell. Transp. Syst. 12 (1), 97–108.
Saruwatari, K., Sakaue, F., Sato, J., 2012. Detection of abnormal driving using multiple view geometry in space–time. In: 2012 IEEE Intelligent Vehicles Symposium (IV), pp. 1102–1107.
Sultani, W., Choi, J.Y., 2010. Abnormal traffic detection using intelligent driver model. In: 2010 International Conference on Pattern Recognition.
Sun, R., Feng, S., Ochieng, W.Y., 2014. An integrated solution based irregular driving detection. ION GNSS 2014.
Toledo-Moreo, R., Bétaille, D., Peyret, F., 2010. Lane-level integrity provision for navigation and map matching with GNSS, dead reckoning, and enhanced maps. IEEE Trans. Intell. Transp. Syst. 11 (1), 100–112.
Tsogas, M., Polychronopoulos, A., Amditis, A., 2005. Unscented Kalman filter design for curvilinear motion models suitable for automotive safety applications. In: Proceedings of 7th IEEE International Conference on Information Fusion, pp. 1295–1302.
Zadeh, L.A., 1965. Fuzzy sets. Inf. Control 8, 338–353.
Zhu, Z., Ji, Q., 2004. Real time and non-intrusive driver fatigue monitoring. In: Proceedings of 7th International IEEE Conference on Intelligent Transportation Systems, ITSC 2004. Washington, DC, United States, 3–6 Oct 2004, pp. 657–662.